4-2-2010

Influence of Cu Diffusion Conditions on the Switching of Cu-SiO_2-Based Resistive Memory Devices

S.C. Puthen Thermadam
Arizona State University

S. K. Bhagat
Arizona State University

T. L. Alford
Arizona State University

Y. Sakaguchi
Boise State University

M. N. Kozicki
Arizona State University

See next page for additional authors

Authors
S.C. Puthen Thermadam, S. K. Bhagat, T. L. Alford, Y. Sakaguchi, M. N. Kozicki, and Maria Mitkova

Influence of Cu Diffusion Conditions on the Switching of Cu-SiO2-Based Resistive Memory Devices

S. C. Puthen Thermadam[1], S. K. Bhagat[2], T. L. Alford[2], Y. Sakaguchi[3], M. N. Kozicki[1], M. Mitkova[3]
[1]Center for Applied Nanoionics, Arizona State University, Tempe, AZ 85287-6206, USA
[2]School of Materials, Arizona State University, Tempe AZ 85287-8706, USA
[3]Department of Electrical and Computer Engineering, Boise State University, Boise, ID 83725-2075, **USA**

Abstract

This paper presents a study of Cu diffusion at various temperatures in thin SiO_2 films. Film composition and diffusion products were analyzed using Secondary Ion Mass Spectroscopy, Rutherford Backscattering Spectrometry, X-ray Diffraction and Raman Spectroscopy methods. We found a strong dependence of the diffused Cu concentration, which varied between 0.8 at.% and 10^{-3} at. %, on the annealing temperature. X-ray diffraction and Raman studies revealed that Cu does not react with the SiO_2 network and remains in elemental form after diffusion. Programmable Metallization Cell (PMC) resistive memory cells were fabricated with these Cu-diffused SiO_2 films as the active elements and device performance is presented and discussed in the context of the materials characteristics.

Key words: compositional characteristics, non-volatile memory, nanoionic devices, silicon dioxide based memory

1. Introduction

There is currently a tremendous drive to develop non-volatile devices which will ultimately replace Flash memory. The requirements demanded of such replacements include high operating speed, non-destructive reading, low energy programming, compatibility with the CMOS process, and low fabrication costs. One very promising solution involves switching based on devices in which solid electrolytes combined with one oxidizable and one inert electrode constitute the active structure. This is the basis of Programmable Metallization Cell (PMC) memory devices. These utilize the reduction of nanoscale quantities of metal ions in the solid electrolyte film to form a metal link between the two electrodes. Due to the electrochemical nature of the process the metal link can be dissolved by application of opposite bias on the electrodes. Devices based on Ge-chalcogenides combined with Ag or Cu, and WO_3 combined with Cu gave promising results in the context of PMC resistance change devices [1-3]. The specific benefits of these devices come from their widely spaced resistance states, low programming voltage/current, possibility for multilevel storage, and high scaling capability. One very important characteristic of these devices is that the memory is non-volatile due to the fact that the data-representing resistance change is caused by the formation of a feature formed from neutral atoms, which do not, of course, display the same leakage-based retention failure mechanisms of charge-based memories. The application of SiO_2 in the active medium of PMC memory elements proved to be a viable alternative to chalcogenide- or transition oxide-based materials [4]. The main advantage of SiO_2-based devices is their ease of integration in CMOS technology, particularly in the back-end-of-line (BEOL) sequence, where the fabrication processes necessary for the device formation are already in use. The initial findings from the characterization of such devices have shown promising results [5]. However, for this material to reach its full potential in this application, the materials must be fully characterized.

There are two intrinsically related aspects of equal importance which need to be addressed in order to achieve performance optimization of SiO_2-based PMC devices; one is to identify which composition gives the best device performance and the other is to determine what processing is necessary in order to produce devices with specific parameters. Critical to this enhanced understanding is a determination of how the Cu interacts with the SiO_2 network, what the distribution of Cu within the SiO_2 film is, and what is the new structure forming after Cu is embedded in the film. SiO_2 has been used as both a dielectric and a barrier in the semiconductor industry for decades and so the diffusion of metals in this material is well understood. From these studies, it is known that Cu has a higher diffusivity in SiO_2 than other metals such as Fe [6], however, Cu solubility in SiO_2 films is still expected to be quite limited. This opens up some challenges for the characterization methods due to the expected low concentration of Cu in the hosting oxide film.

In our previous work we noted that the introduction of Cu by photodiffusion (as used in the formation of Ge-chalcogenide solid electrolytes) is not favored [4] due to the specific bond organization and strength of the chemical bonding in SiO_2. Other options are thermal diffusion and ion implantation which have been successfully applied to the introduction of Cu in SiO_2 films [6,7]. We have used thermal diffusion since this method of metal introduction is more acceptable than Cu ion implantation in mainstream semiconductor processing due to the lack of readily available implant sources. In this article we discuss the results of Cu diffusion into SiO_2 films at different annealing temperatures and times. Data is presented regarding the new structure forming after Cu diffusion in the hosting SiO_2 film and its depth distribution using a variety of characterization techniques. These materials characterization results are related to the performance of PMC devices prepared under different conditions

This work is aimed at giving a general perspective of the materials options that could be used in devices and to be a model for the explanation of their performance.

2. Experimental

2.1. Materials stack preparation

All materials characterization experiments were performed on blanket films of Cu doped SiO_2 on a TiN/Si substrate. The TiN layer formed a diffusion barrier for Cu and prevented Cu diffusion into the Si substrate. In this manner we avoided the opportunity for contact between the diffused Cu and the pure Si substrate, which could lead to additional reactions that would complicate the interpretation of the experimental results. The SiO_2 and Cu films were deposited using a Torrvac VC-320 electron beam evaporator at an average evaporation pressure of $3x10^{-6}$ Torr and 0.2 nm/s deposition rate. The stack sequence for the material characterization samples top to bottom was as follows: 800 nm SiO_2; 400 nm Cu; 600 nm SiO_2; 80 nm TiN. The top SiO_2 layer was used to prevent the oxidation of the Cu film during the thermal processing of the samples. The high temperature thermal doping of SiO_2 with Cu was carried out in a Lindberg Tube Furnace in an N_2 (flowing) ambient. The stacks were split in several groups, each one annealed at 560 ^oC, 660 ^oC, or 720 ^oC for 15 min, 1 hour or 2 hours respectively. After high temperature processing, the top SiO_2 layer was etched off using 20:1 BOE. To exclude the influence of the top Cu film, following the thermal processing it was dissolved with a standard Cu etchant 49-1 from Transene Company, Inc., a citric acid based etchant with an estimated etch rate of 22 Å/s at 30^oC. Figure 1 represents the stack used for this study and the layer structure after dissolution of Cu. This structure was then analyzed to provide data regarding the Cu diffusion in the SiO_2 film.

2.2. Device preparation

A schematic of a typical PMC device structure is shown in Figure 2. A 100 nm thick tungsten layer was deposited using a chemical vapor deposition (CVD) process on thermally grown SiO_2 on a Si substrate. 100 nm of silicon nitride was deposited on top of this tungsten layer using CVD and vias which define the active device regions were patterned using optical lithography and etched using RIE to expose the bottom tungsten film. The via diameters varied from 5 µm - 0.18 µm. Probe windows to contact the tungsten bottom electrode were opened up using another lithography and etch process. 15 nm of SiO_2 and 40 nm of Cu were deposited on this patterned substrate under similar deposition conditions as the samples used for material characterization. The top electrode (Cu) for electrical probing was then patterned by a lift-off process. A protective layer of SiO_2 was deposited on top of the Cu electrode to prevent its oxidation during the thermal treatment. This layer was etched off using 20:1 BOE after the annealing process. The annealing conditions of the devices were at 560^oC, 660^oC and 720^oC for 15 minutes in N_2 (flowing) ambient.

2.3. Materials characterization

X-ray diffraction analysis (XRD) was used to identify phases formed in the as-deposited and annealed samples. One degree glancing scan XRD was performed using a Phillips X'pert MPD diffractometer. Cu Kα radiation was used as the source and samples were investigated over an angle range of 5-100^o with 0.01^o step size and 1 second time per step. The voltage and current settings were 45 kV and 40 mA respectively. In the glancing scan XRD analysis, the angle of source from the sample surface is fixed at a lower value (1^o in our case) while the detector moves in the usual manner. In a θ-2θ geometry scan, the angle of incidence is always equal to the angle of exit. Hence, at higher angles to detect higher plane reflections, the penetration depth of x-rays may be greater than the thickness of thin film, resulting in unwanted substrate peaks and noise. Glancing angle X-ray diffraction reduces this to a significant extent, however, it provides a larger interaction volume within the studied thin film as compared to θ-2θ geometry scan.

Backscattering analysis was performed using a 2.0 MeV He^{++} ion beam at a tilt of 8^o in a General Ionex Tandetron accelerator. A tilt of 50^o was used as well to improve depth resolution and verify the Cu distribution in the film. A computer program RUMP was used to simulate RBS spectra [8].

SIMS analysis was done in a Cameca IMS 3f magnetic-sector SIMS instrument. O^- ions at 17 keV and 50 nA ion current were used as the primary ions since their application minimizes the charging problems in the SiO_2 films. Positive ion mass spectra and depth profile were obtained. The depth scale of the depth profile was determined from Tencor stylus profilometer linescan measurements across the sputter crater.

Raman spectra were recorded using a Raman spectroscopic system, Horiba Jobin Yvon T64000, in backscattering geometry. The 441.6 nm laser line of the helium-cadmium continuous wave laser (Kimmon Koha Co., Ltd. IK5752 I-G) at a power of 83 mW was used for the excitation at an acquisition time of 1 min. The signal was analyzed with a thermoelectrically cooled CCD camera.

2.4. Device characterization

The switching characteristics of the devices annealed at different temperatures were studied using slow voltage sweeps. These were applied by connecting the device electrodes via tungsten probes held in a micromanipulator in a probe station to a semiconductor parameter analyzer (Agilent 4155C). Voltage double sweeps were used, starting at -0.75 V (copper electrode negative and tungsten electrode positive), sweeping to 1.5 V (copper electrode positive and tungsten electrode negative), and sweeping back again to -0.75 V. For a typical PMC device with oxidizable and inert electrodes, this double sweep should have put the devices in an erased (high resistance) state to start with, written them with the positive bias, and then erased them with the final negative bias, however, as we will see later, some devices in this study showed unipolar (the same polarity for both write and erase) characteristics. The compliance current setting in the 4155C was used to limit the current passing through the device once the device was written.

3. Results

The results regarding the amount of copper diffused into the SiO_2 films measured by SIMS are shown in Figure 3. Concentration is calculated with respect to silicon by assuming that the ion yield of Cu+ and heavily oxidized silicon is approximately the same (within a factor of 5). The ratio of Cu+/Si+ is then taken as the concentration of Cu^+. The interface profile is not characterized by a sharp difference between the two films which is an indication that the interdiffusion starts even during the time of the copper film deposition. There is approximately three orders of magnitude difference in the amount of diffused Cu for the two temperatures studied; approximately 0.8 at. % for diffusion at 720^{o}C and around 10^{-3} at. % for diffusion at 560^{o}C. The spectra follows the standard Cu^+_{63} and Cu^+_{65} isotope ratio nicely.

Figure 4 a) and b) show the RBS spectra taken from a Cu-doped-SiO_2/TiN structure. The amount of Cu diffused in the SiO_2 film after annealing at 560^{o}C could not be detected in this experiment since it is below the sensitivity limit of the technique. For the sample annealed at 720^{o}C for 15 minutes the experimental curve shows a faint signal near channel 300 in addition to the major Si and oxygen peaks. Ti also produces peaks close to this region. Furthermore, we see two more peaks close to channel 400. Since the signals from Cu and Ti are very close, fine calibration is needed for a detailed description of the composition studied. We suggest that the signal at channel 300 comes from Ti under the SiO_2 film, and the wide signal at channel 320 belongs to Cu at the SiO_2/TiN interface. Given that the width of the Cu peak is greater than the system energy resolution (~ 7 channels), this is an indication that Cu exists at the interface with the TiN. The signal at channel 430 reveals a surface nature and we assign it to the Cu that is part of the first diffused quantity.

Figure 5 shows the XRD data collected from our films. Among the numerous peaks that are characteristic for all the participating elements and compositions we can observe those of Cu which are the only peaks related to this element, i.e., our results show that Cu remains in elemental form during processing. The intensity of these peaks rises with increasing annealing temperature.

The Raman results in Figure 6 a) and b) show in a most impressive manner the dependence on the film's characteristic upon the annealing conditions. The Raman modes intensity characteristic for the SiO_2 films decreases with increasing annealing time or temperature and no new features occur with the extension of the annealing conditions. Note specifically the strong decrease of the Raman activity with temperature caused by annealing at 660^0C. The films are characterized by a relatively sharp band at 440 which arises from symmetrical Si-O-Si stretching modes principally involving motion of the oxygen atom. The modes at 510 and 640 cm^{-1} occur from symmetric stretching modes of small-ring configurations in the three-dimensional random network [9]. There are two very weak features at 1060 and 1190 cm^{-1} which are not shown because of their low relevance and for a clearer presentation of the modes at lower wavelengths. Note that Cu is not expected to appear on these spectra since it is Raman silent [10] but its presence in the films can be inferred from the reducing Raman activity of the hosting film due to its increased conductivity because of the Cu inclusion. If Cu oxidation occurred during the annealing process, features could be expected in the 290 – 624 cm^{-1} region [11].

Figures 7 a) and b) show representative I-V characteristics of devices formed by films annealed at 720^oC and 660^oC, respectively. Note that both unipolar and bipolar switching is possible. The progression of the voltage sweep is shown with the help of numbered arrows, indicating the direction of the voltage sweep and the sequence of the events during the sweep. The device conducts a current equal to the compliance current, 25 µA in this case, when it written or switched ON at the switching threshold voltage. The device conducts negligible current once it is erased or switched OFF. In Figure 7 a), which shows symmetrical unipolar switching (both write and erase in either polarity), the device follows a sequence of OFF(4)-ON(5)-OFF(9)-ON(12), (the numbers in parentheses refer to the corresponding numbered arrow in the figure). In the case of the bipolar switching shown in Figure 7 b) it follows the sequence ON(3) – OFF(8). In both cases, three consecutive voltage sweeps are shown. It should be noted that the switching threshold is higher (~0.5 V) for the bipolar switching device. The switching threshold shows a close dependence on the annealing temperature and decreases for samples with films annealed at higher temperature as shown in Figure 8. We show the threshold voltage occurring after the first sweep since it gives a better understanding of the influence of the thermal doping alone, because switching in the subsequent sweeps could be influenced by a change in the material caused by the previous voltage sweep. Indeed, multiple sweeps show that switching occurs at lower threshold voltage after the initial sweep as shown in Figure 9.

4. Discussion

We will start our discussion with some remarks about the host SiO_2. Although this material has been widely studied, there is little data regarding SiO_2 films formed by e-beam evaporation, which could be due to the fact that this method of film formation is not typically used in conventional Si processing. The films are amorphous as revealed by the wide Raman and XRD features. In our case, the e-beam evaporated film was deposited over a polycrystalline TiN film. Hence, one can expect an increased number of defects compared to a thermal oxide grown on single crystalline Si. Indeed the appearance of the 'defect Raman bands' at 510 and 640 cm^{-1} on Figures 6 a) and b) are direct evidence of the high disorder of the structure [9]. This disorder will result in the formation of voids within the oxide film which are favorable for the diffusion process and almost certainly play a role in the switching process (discussed later).

Cu has a relatively high diffusivity in SiO_2 and isotope tracking analysis shows that it can penetrate far into an SiO_2 film [12,13]. Moreover, this latter study has shown that Cu can move bidirectionally (in and out of the oxide film) which is an indication that it does not chemically react with the SiO_2 matrix. This result is in a good agreement with the RBS data obtained in our study where we identified Cu at the SiO_2 / TiN interface as well as near the Cu/SiO_2 surface, which is also a sign of the high mobility of Cu in the SiO_2 film. A similar distribution has also been reported by Sun at al. [14].

When we discuss the thermal diffusion of Cu into the SiO_2 film, we have to consider the temperature-related changes occurring within the hosting material. It has been found that by increasing the temperature, electronically excited states are accumulated in the skeletal Si-O bond system as well as by formation of associates in the cationic and anionic sublattices [15]. The net result of this is that an additional energy reservoir appears which is favorable for the diffusion process at increased temperatures. Moreover, the dynamic exchanges in the structure of the hosting SiO_2 film leads to formation of films with increased porosity. It is for this reason, and the others given above, that the Cu diffusion is significantly accelerated at higher temperature. We see evidence for this increased diffusivity in the Raman spectra.

Next, we have to consider the fact that we are dealing with a multi-layer structure which can result in significant thermal stress and residual strain-induced effects. For example, it has been noted that the void formation rate in SiO_2 with a Cu metal film deposited on top increases with an increase in temperature [16]. In general, due to the difference in the thermal expansion coefficients of the different films in the stack, significant stresses are expected to occur in the hosting medium. Indeed, the slight shift of the Raman modes compared to the relaxed SiO_2 [9] is an indication of the strain occurring in the material. Stress- or point-defect relaxation can occur at any of the studied temperatures and this is an additional reason for enhancement of the diffusion process. Pan et.al. [7] noted an optimum annealing condition around 600^0C to improve indentation induced precipitation. Our results show a drastic decrease in the intensity of the Raman breathing modes after annealing at 660^0C which is indication for enhanced Cu diffusion at this temperature. The same Cu-related trend is noted for the threshold voltage for the first sweep which is considerably lower in the devices annealed at 660^0C compared to those annealed at 560^0C. Our assumption is that the latter devices have higher switching thresholds due to the lower concentration of Cu introduced into the SiO_2 matrix, while for those annealed at 660^0C there is well expressed nanoparticles precipitation and growth [7] which contribute to devices switching at lower threshold voltage.

From the XRD results, we conclude that Cu does not react with the constituents of the SiO_2 network and remains in elemental form when diffused into the dielectric film, leaving most Si atoms in a configuration with four oxygen bridging atoms. The lack of formation of CuO or other oxides, silicates or silicides was also demonstrated by our Raman spectra. Our results are in a good agreement with the data reported by Dallaporta et. al. [16]. Moreover the Cu transport that we will discuss next is also suggestive that Cu remains free into the SiO_2 matrix. These results contradict the data described by Cao et. al. [17] who suggest the formation of Cu_3Si in their study of the diffusion processes in the Cu/SiO_2/Si system at temperatures over 450^0C. We believe that their result is a consequence of the fact that Cu, due to its relatively high diffusivity, has reached the SiO_2/Si interface as discussed earlier and formation of silicides is possibly due to Cu reaction with pure Si.

Applying our newly-gained knowledge of material characteristics to the electrical performance of the PMC devices studied, we can better comprehend their operation. Since the concentration of Cu is quite low in the as-diffused glass in all cases, there will be insufficient metal to significantly influence the resistivity of the material and hence the resistance of the device will be relatively high. When a positive bias is applied across the Cu-doped films via a Cu electrode, which can be regarded as a supplier of Cu^+, accelerated diffusion of Cu^+ will occur due to the reduction in the activation energy [18, 19] and the presence of the large number of voids and pathways in the host glass, as discussed above. One can conclude that resistance reduction in the devices is due to the addition of Cu into the void-filled random network of the hosting glass, where it joins the existing Cu to form conducting Cu-rich pathways. An opposite bias (Cu electrode negative) takes this added material out of the glass and back to the Cu electrode by the same process, returning the device to its high resistance state.

As noted above, annealing at higher temperatures results in much more Cu being introduced into the SiO_2 due to the larger number of voids formed compared to the lower temperature annealing cases. It is likely that this same void-rich structure will also allow Cu to enter the film more easily under positive bias. We suggest this is the reason that devices formed from material diffused at higher annealing temperature have a lower threshold voltage. This chemically stable but “open” structure facilitates the transport of Cu and at the same time does not create conditions for the chemical stabilization of Cu as oxide within the glass. We also believe that the fact that Cu does not form chemical bonds with the SiO_2 host is the reason for the fluctuations in the threshold voltage values from device to device obtained for the same programming conditions (see Figure 8) and during multiple sweeps (Figure 9), as the unbound Cu can readily be thermally (during processing) or electrically (during programming) redistributed within the film. Note also that the multiple sweeps result in minimum threshold dispersion at an annealing temperature of 660^0C (Figure 8) and we therefore believe this is close to the optimal conditions for solid electrolyte formation. There is a general trend of decreasing switching threshold voltage with consecutive sweeps. This could be a conditioning effect, whereby less Cu ions have been removed from the SiO_2 during the erase than those that have been introduced during the write.

The appearance of devices processed at higher temperature which exhibit both symmetrical unipolar and non-symmetrical bipolar switching can be understood by considering the RBS results (Figure 4b). We believe that this effect is related to the fact that in some instances, Cu diffuses across the entire thickness of the SiO_2 film to the SiO_2/W interface, thus forming a symmetrical Cu-SiO_2-Cu structure which leads to programming or erasing in either direction. Note that in such devices, the erase mechanism could involve the thermal dissolution of the conducting Cu filaments due to Joule heating, rather than an electrochemical oxidation of the metal. In the case of bipolar switching, Cu remains in the SiO_2 volume and the devices only program and erase under Cu electrode positive and Cu electrode negative bias respectively, as expected for non-symmetric device structures.

5. Conclusions

In this work we provide materials characterization of Cu-doped SiO_2 films which are applied as the active film (solid electrolyte) in PMC devices. The main results are as follows:

The thermal diffusion product for Cu films on evaporated SiO_2 layers is an oxide matrix with unreacted Cu atoms embedded in it. This result has been confirmed by XRD and Raman measurements.

Based on the characterization data, we propose that Cu diffusion in SiO_2 occurs via channels and voids formed in the glassy network, the presence of which increases with an increase in the annealing temperature and results in higher Cu concentration than expected for thermally-activated diffusion alone at higher temperature.

There is a close relationship between the threshold voltage of the PMC devices and the annealing conditions for Cu diffusion. The lowest threshold voltage is obtained for material diffused at the highest temperature, probably due to the higher number of voids present.

The fact that Cu does not form chemical bonds with the SiO_2 network leads to fluctuations in the switching threshold voltage following processing and programming. The smallest fluctuations are observed with films annealed at 660^0C.

During multiple sweeps, there is a drift of the threshold voltage to lower values which is probably related to some Cu ions remaining in the solid electrolyte, i.e., less ions are removed from the SiO_2 during the erase than have been introduced during the write.

Due to the high diffusivity of Cu in SiO_2, there is a chance that higher annealing temperatures can result in the formation of devices with a Cu/SiO_2/Cu structure due to the diffusion of Cu through the entire volume of SiO_2 and accumulation on the interface with the bottom electrode. These devices tend to show symmetric unipolar switching. Non-symmetric bipolar switching is exhibited by devices with a Cu/SiO_2/W structure, more typical of moderate to lower temperature annealed devices.

References:

M.N. Kozicki, M. Park M. Mitkova, IEEE Trans. on Nanotechnology 4 (2005) 331.

M.N. Kozicki, M. Mitkova, M. Park, M. Balakrishnan, C. Gopalan – *Superlat. & Microstr.*, 34 (2004) 459.

C. Gopalan, M. N. Kozicki, S. Bhagat, C. Powelait, T. Alford, M. Mitkova, J. Non-Cryst. Sol 353 (2007) 1844.

M. Balakrishnan, S. C. P. Thermadan, M. Mitkova M. N. Kozicki IEEE Proceedings 2006 Non-volatile Memory Technology Symposium, 5-8 November 2006 San Mateo, California, USA p. 104.

C. Schindler, S.C. Puthen Thermadam, R. Waser and M.N. Kozicki, IEEETrans. Electr. Devices 54 (2207) 2762.

B. Johannesen, P. Kluth, C. J. Glover, G. J. Foran, M. C. Ridgway, Nucl. Instr. Phys. Res. B 242 (2006) 113.

J. Pan, H. Wang, Y. Takeda, N. Umeda, K. Kono, H. Amekura, N. Kishimoto, Nucl. Instr. Phys. Res. B 257 (2007) 585-588.

L.R. Doolittle, Nucl. Instrum. Methods Res. B 9 (1985) 344.

R. J. Hemley, H. K. Mao, P. M. Bell, B. O. Mysen, Phys. Rev. Lett. 57 (1986) 747.

Y. S. Gong, C. Lee, C. K. Yang, J. Appl. Phys. 77 (1995) 5422.

J. F. Xu, W. Ji, Z. X. Shen, W. S. Li, S. H. Tang, X. R Ye, D. Z. Jia, X. Q. Xin, J. Raman Spectroscopy 30 (1999) 413.

J. D. McBrayer, R. M. Swanson, T. W. Sigmon, J. Electrochem. Soc. 133, (1986)1242.

S.-W. Lee, Y.-H. Kim, K.-S. Kim, B.-S. Hong, B.-Y. Lee, J. of the Korean Phys. Soc. 48 (2006) 1548.

Y.-M. Sun, S. Y. Lee, A. Lemonds, J. Lozano, J.-P.Zhou, J. G. Ekerdt, J. M. White I. Imesh, Surf. Interface Anal. 32 (2001) 79.

V. B. Kopylov, K.A. Aleksandrov, E. V. Sergeev, Russ. J. of Gen. Chem. 78 (2008) 868.

H. Dallaporta, M. Liehr, J. E. Lewis, Phys. Rev. B 41 (1990) 5075.

Cao Bo, Li G.-P., Chen X.-M., Cho S.-J., Kim H., Chin. Phys. Lett. 25 (2008) 1400.

I. Fisher, M. Eizenberg, Thin Solid Films, 516 (2008) 4111.

Y. Shacham-Diamand, A. Dedhia, D. Hoffstetter, W. G. Oldham, J. Electrochem. Soc. 140 (1993) 2427.

Figure captures:

Fig. 1. Schematic of the blanket stack used for materials characterization.

Fig. 2. Schematic of the PMC device structure used for electrical testing of the Cu-SiO_2 films.

Fig.3. SIMS profiles of Cu in SiO_2 films for different diffusion conditions.

Fig. 4. RBS spectra of Cu doped films after annealing at 560^{o}C for 2 hours and at 720^{o}C for 15 minutes.

Fig. 5. X-Ray diffraction data from sample with no thermal doping of Cu and samples in which thermal doping was done at 560^{o}C for 2 hours and 720^{o}C for 15 minutes respectively.

Fig. 6. Raman spectroscopy data for a Cu doped SiO_2 film approximately 650 nm thick. SiO_2 was doped with Cu by annealing at a) 560^{o}C for 15 min, 1 hour and 2 hours b) 1 hour at 560^{0}C, 660^{0}C and 720^0 C

Fig. 7. I-V device characteristics; a) Device annealed at 720^{0}C showing low switching threshold for unipolar switching; b) Device annealed at 660^{0}C showing higher thresholds and bipolar switching.

Fig. 8. Switching thresholds of the first voltage sweep on the device after processing.

Fig. 9. Threshold variation with subsequent voltage sweeps.

Fig. 1.

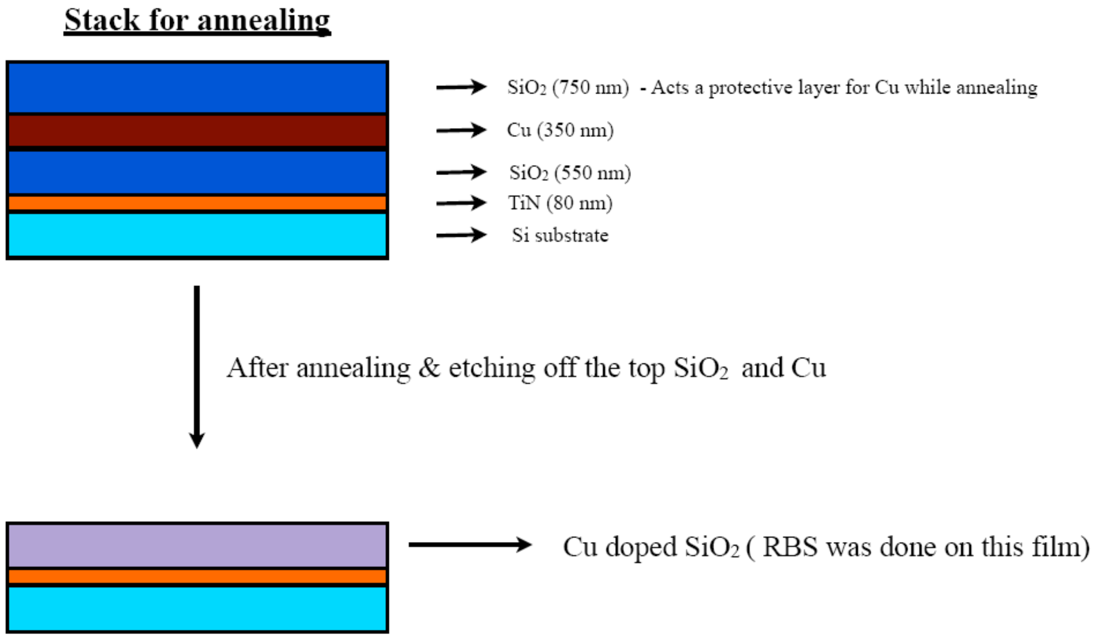
Stack for annealing
SiO2 (750 nm) - Acts a protective layer for Cu while annealing
Cu (350 nm)
SiO2 (550 nm)
TiN (80 nm)
Si substrate
After annealing & etching off the top SiO2 and Cu
Cu doped SiO2 (RBS was done on this film)

Fig. 2.

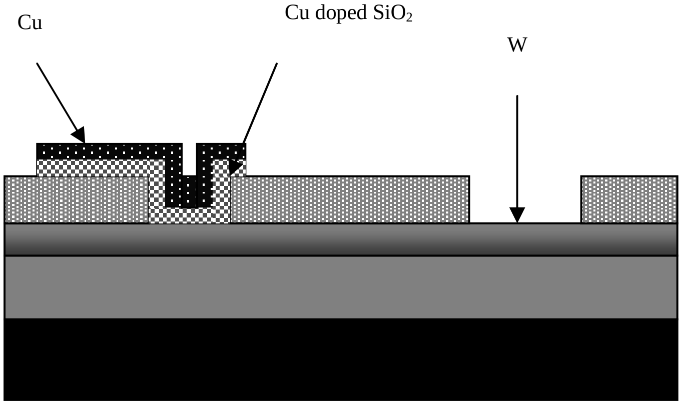

Fig. 3.

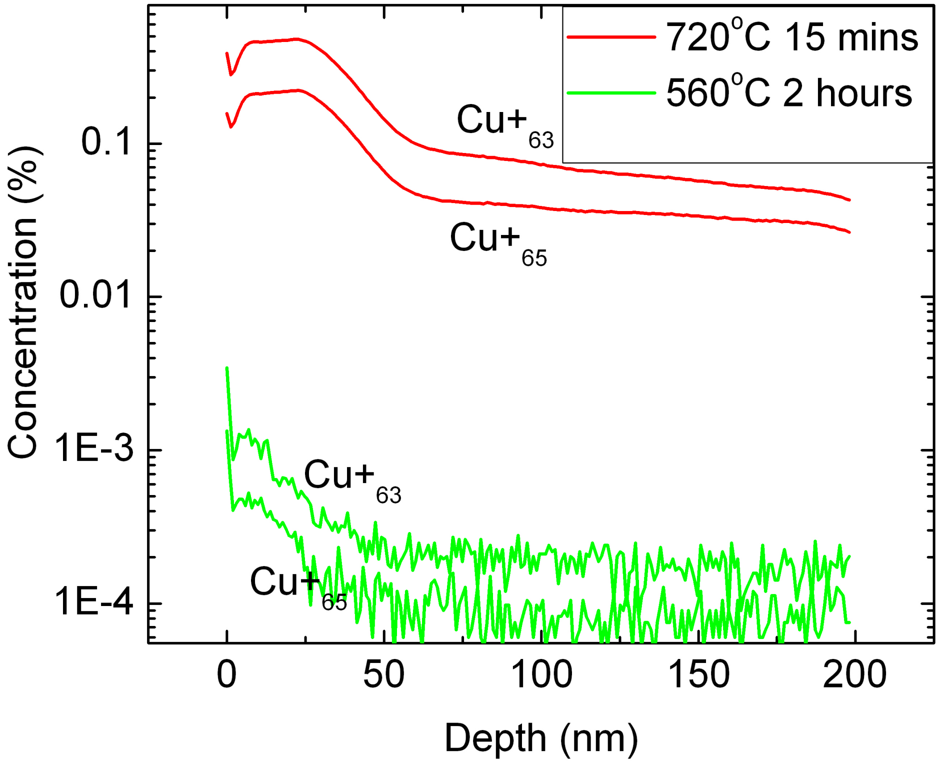
720°C 15 mins
560°C 2 hours
Cu+63
Cu+65
Cu+63
Cu+65
Concentration (%)
0.1
0.01
1E-3
1E-4
0
50
100
150
200
Depth (nm)

Fig. 4 a

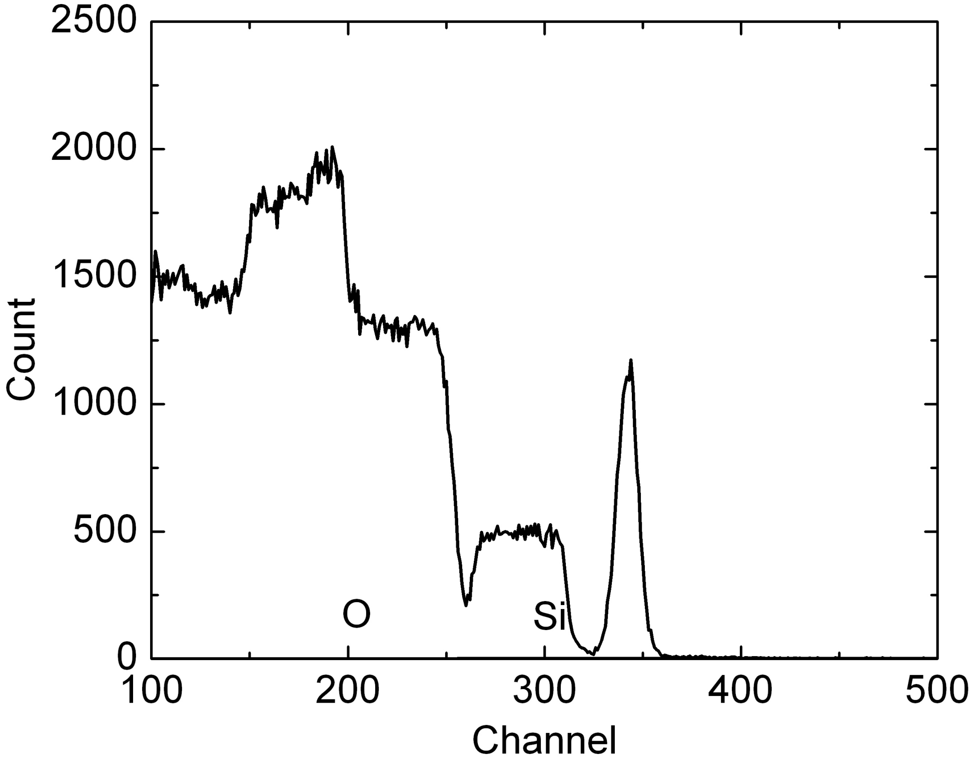
2500
2000
1500
1000
500
0
Count
100
200
300
400
500
Channel
O
Si

Fig. 4 b.

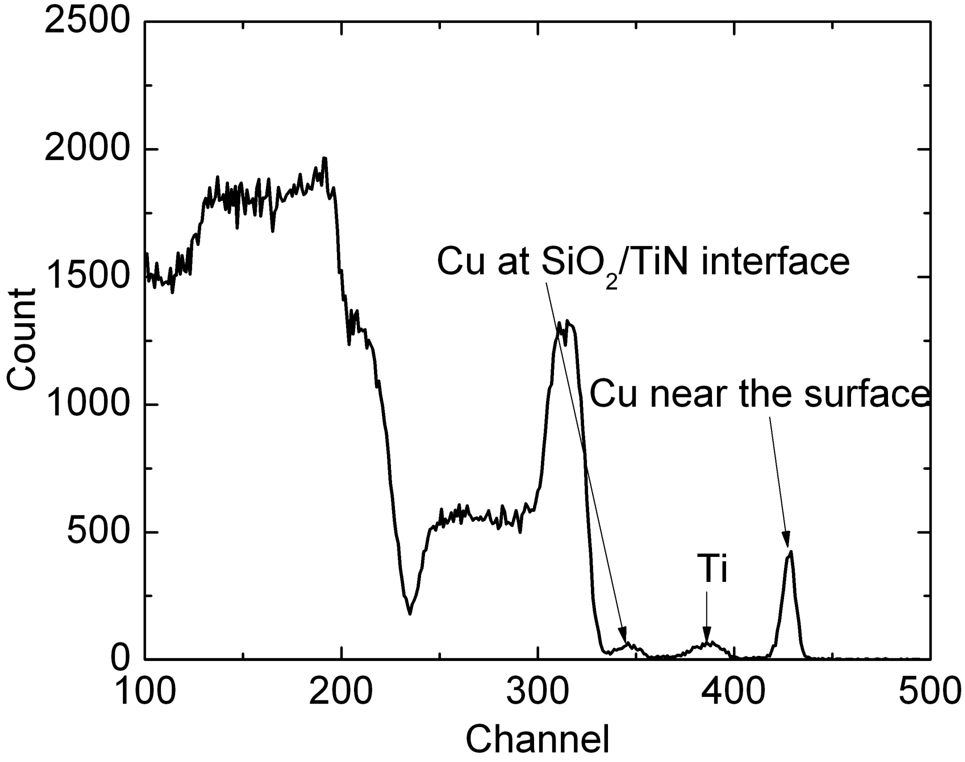
2500
2000
1500
1000
500
0
Count
100
200
300
400
500
Channel
Cu at SiO2/TiN interface
Cu near the surface
Ti

Fig. 5.

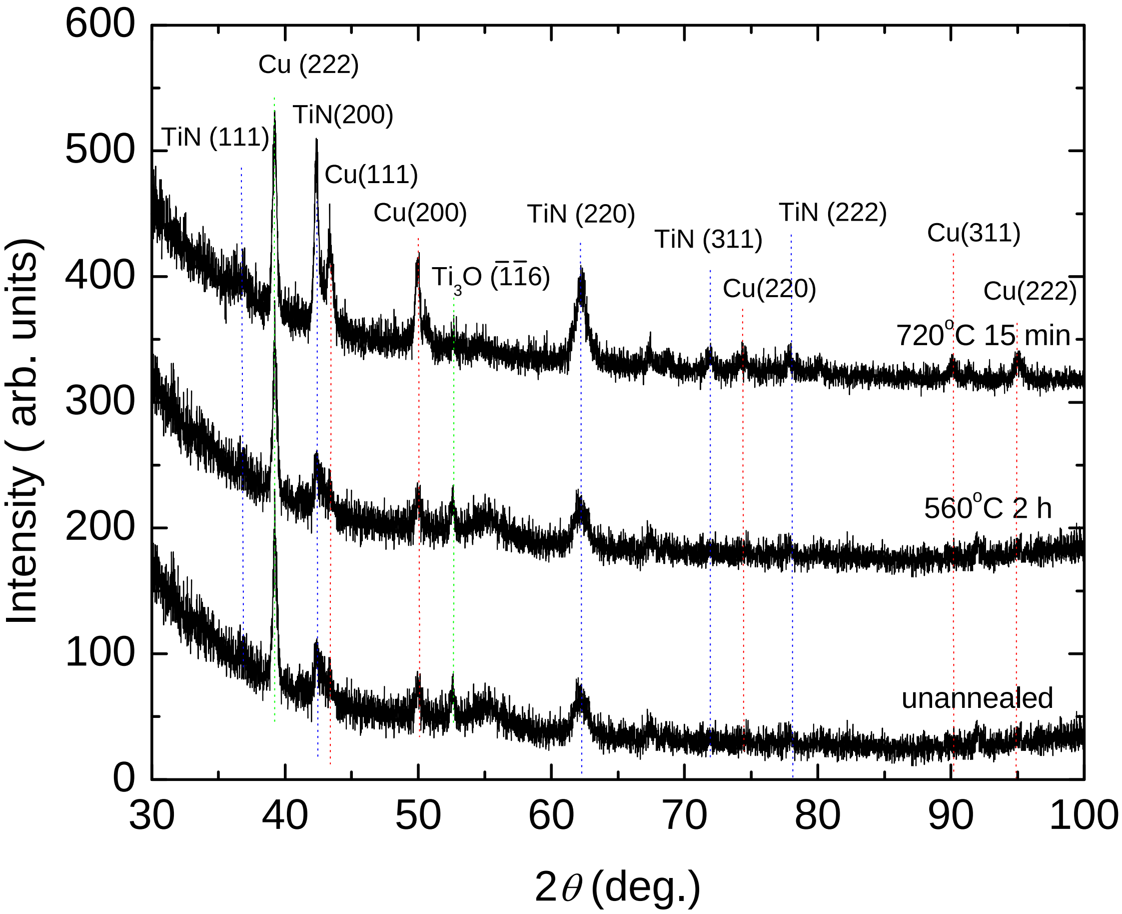
Cu (222)
TiN(200)
TiN (111)
Cu(111)
Cu(200)
TiN (220)
TiN (311)
TiN (222)
Cu(311)
Ti$_3$O ($\bar{1}\bar{1}6$)
Cu(220)
Cu(222)
720°C 15 min
560°C 2 h
unannealed
Intensity (arb. units)
0
100
200
300
400
500
600
30
40
50
60
70
80
90
100
2θ (deg.)

Fig. 6. a

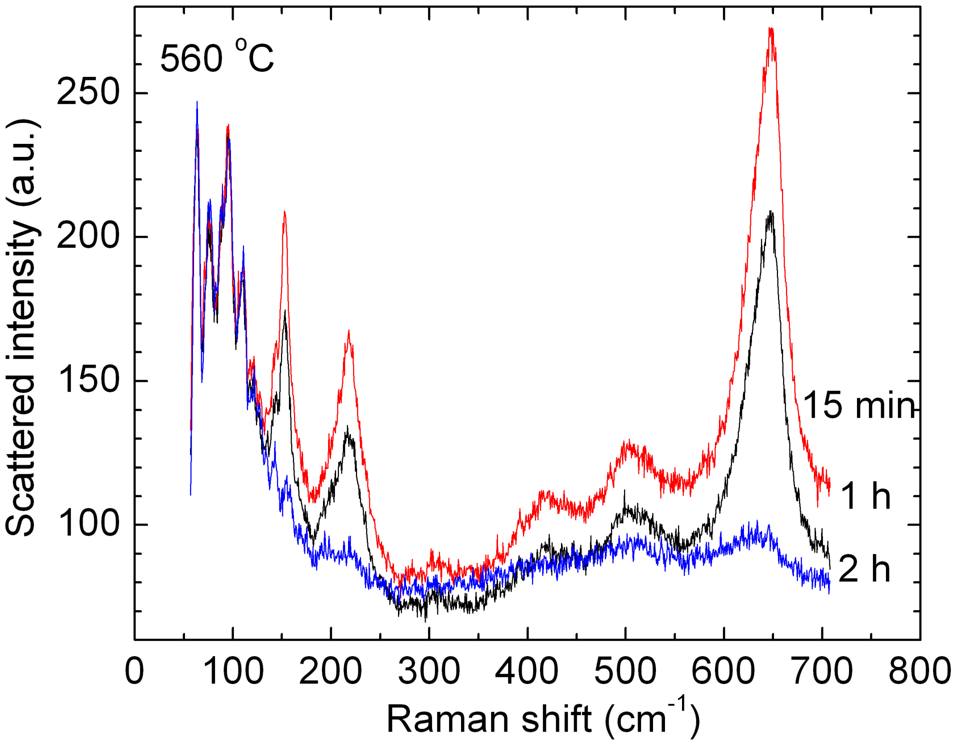
560 °C
Scattered intensity (a.u.)
250
200
150
100
0
100
200
300
400
500
600
700
800
Raman shift (cm^{-1})
15 min
1 h
2 h

Fig. 6 b

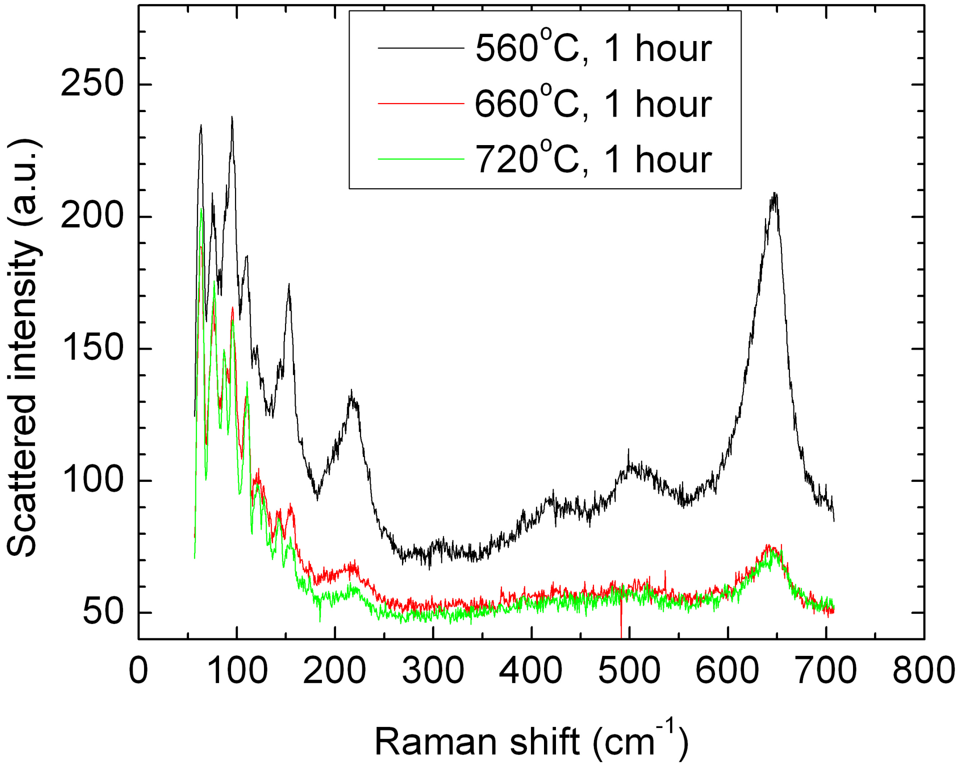
560°C, 1 hour
660°C, 1 hour
720°C, 1 hour
Scattered intensity (a.u.)
50
100
150
200
250
0
100
200
300
400
500
600
700
800
Raman shift (cm^{-1})

Fig7a

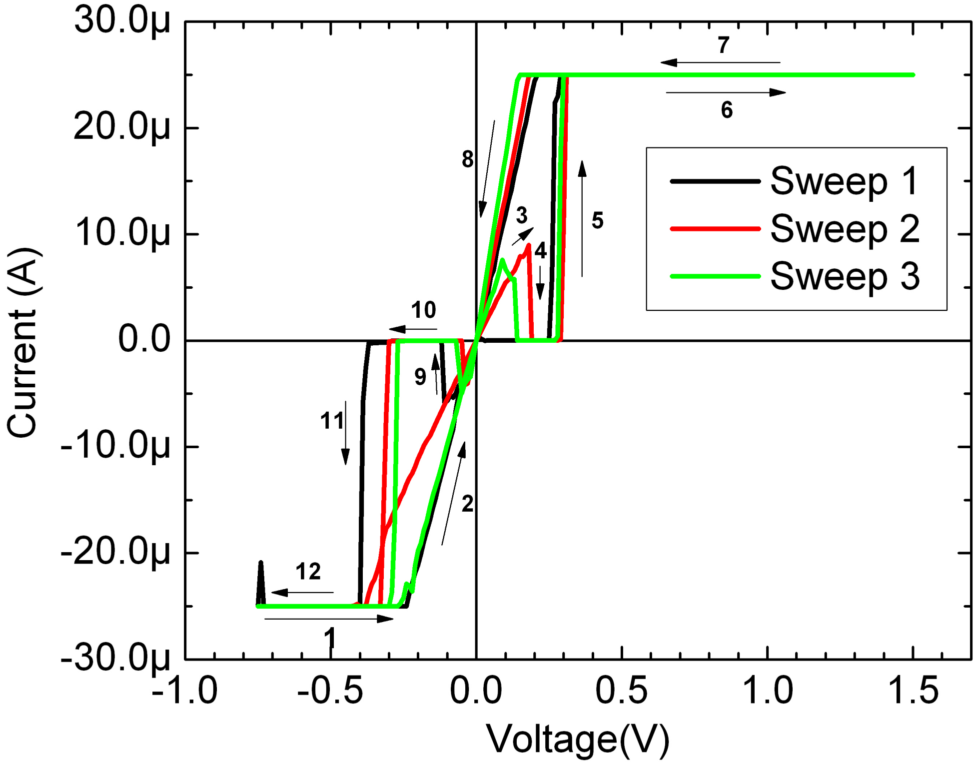
30.0μ
20.0μ
10.0μ
0.0
-10.0μ
-20.0μ
-30.0μ
Current (A)
-1.0
-0.5
0.0
0.5
1.0
1.5
Voltage(V)
Sweep 1
Sweep 2
Sweep 3
1
2
3
4
5
6
7
8
9
10
11
12

Fig 7b

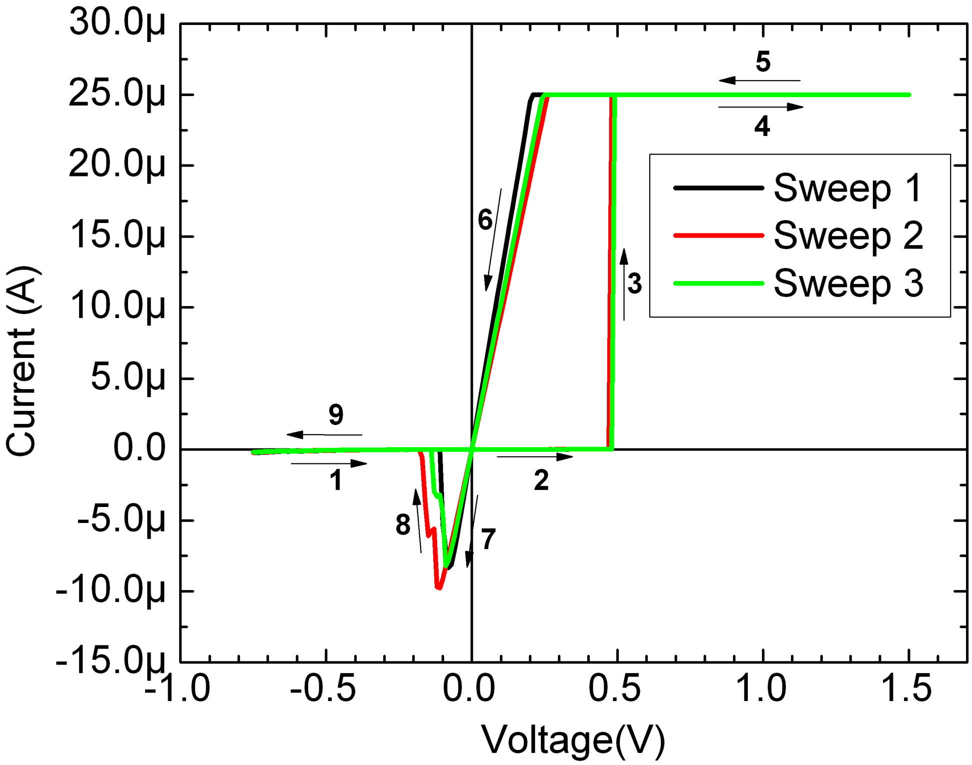
30.0µ
25.0µ
20.0µ
15.0µ
10.0µ
5.0µ
0.0
-5.0µ
-10.0µ
-15.0µ
Current (A)
-1.0
-0.5
0.0
0.5
1.0
1.5
Voltage(V)
Sweep 1
Sweep 2
Sweep 3
1
2
3
4
5
6
7
8
9

Fig. 8.

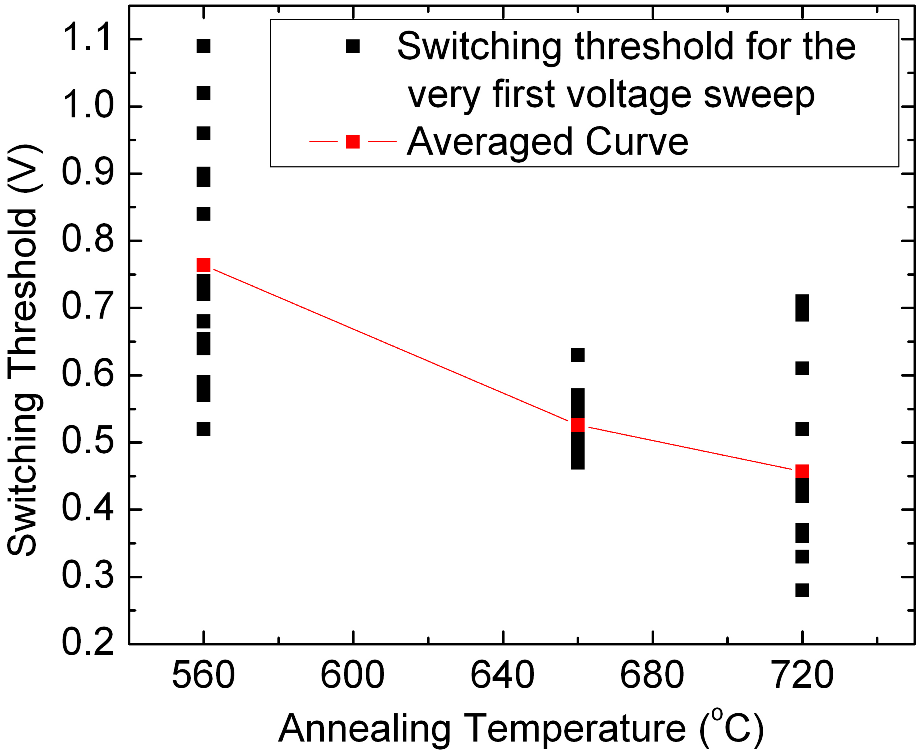
Switching Threshold (V)
1.1
1.0
0.9
0.8
0.7
0.6
0.5
0.4
0.3
0.2
560
600
640
680
720
Annealing Temperature (^{o}C)
Switching threshold for the very first voltage sweep
Averaged Curve

Fig. 9.

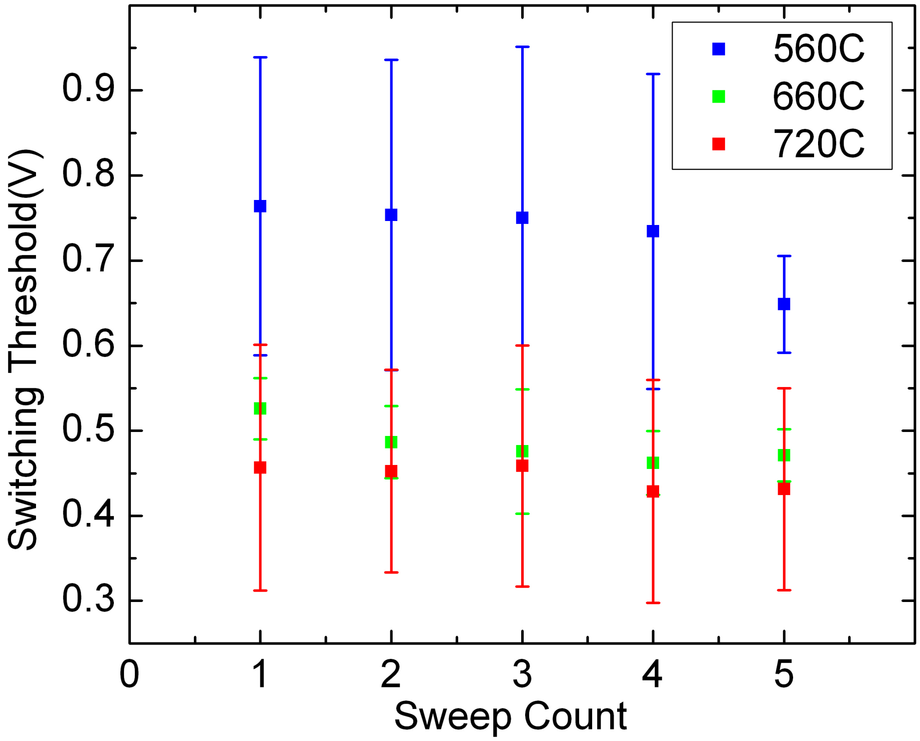
560C
660C
720C
Switching Threshold(V)
0.3
0.4
0.5
0.6
0.7
0.8
0.9
0
1
2
3
4
5
Sweep Count